

MODELING AND SIMULATIONS OF MOVING DROPLET IN A RAREFIED GAS

S. TIWARI, A. KLAR, G. RUSSO

Abstract. We study a liquid droplet moving inside a rarefied gas. In other words, we consider a two phase flow with liquid and rarefied gas phases and an interface between the two phases which deforms with respect to time and space. The gas phase is modeled by the BGK model of the Boltzmann equation. The liquid phase is modeled by the incompressible Navier-Stokes equations. Interface boundary conditions for the liquid and gas phases are presented. The BGK model is solved by a semi-Lagrangian scheme with a meshfree reconstruction procedure. A similar meshfree particle method is used to solve the incompressible Navier-Stokes equations for the liquid phase. To validate the coupled solutions of the BGK model and the incompressible Navier-Stokes equations, we have compared the results of the BGK model and the incompressible Navier-Stokes equations, with those of the Boltzmann and the incompressible Navier-Stokes equations, where the Boltzmann equation is solved by a DSMC method. Results in $1D$ and $2D$ physical spaces are presented.

Keywords. Boltzmann equation, Rarefied gas, BGK model, Particle method, Semi-Lagrangian method, Least squares, Incompressible Navier-Stokes equation, Two-phase flow

MSC2020: 35J15, 76D05, 76P05, 76T10, 65C05, 65M99

1. Introduction. In the past few years liquid-gas flows in micro-nano scale geometries have been quite popular due to the rapid developments in micro-nanofluidics. Some experiments have been performed, where liquid and gas is studied in nanochannels [11, 14, 16]. In such small scale geometries the Knudsen number, i. e. the ratio of the mean free path of the particles and the characteristic length, of these flows are quite large such that the Boltzmann equation is necessary to model the gas phase. For liquid flows the incompressible Navier-Stokes are sufficient to model the liquid phase. Direct Simulation Monte Carlo (DSMC) methods [1, 13] are widely used to solve the Boltzmann equation. In [21] we have presented the coupling of the gas and liquid phases, where the Boltzmann equation is solved by a DSMC method for the gas phase and the incompressible Navier-Stokes equations are solved by a meshfree particle method for the liquid phase. In [21] the coupled solutions of the Boltzmann and the incompressible equations are compared with those of the compressible and incompressible Navier-Stokes equations in $1D$ as well as in $2D$ cases, where in $2D$ only stationary case for a bubble without deformation is studied. DSMC methods are suitable for high speed and stationary flows, however for low speed and non-stationary flows the inherent statistical fluctuations dominate the flow fields and is hard to predict them. In small scale geometries normally flows are low speed flows. In order to get rid of the statistical noises, we employ a deterministic approach for simplified model, like the Bhatnager-Gross-Krook (BGK) model for the Boltzmann equation. Several works have been reported to solve moving rigid objects immersed in a rarefied gas flows, where the BGK model is solved by deterministic approaches [6, 7, 17, 19, 22]. In this paper we extend earlier works presented in [22], where we replace a moving rigid body by a moving liquid droplet, where a rigid body motion was obtained by solving the Newton-Euler equations. We solve the incompressible Navier-Stokes equations for the liquid phase. The interface boundary conditions in the liquid-gas phases are different from the rigid-gas phases. For liquid-gas interactions in $2D$, local deformations of the liquid droplets have to be considered. Since the droplet moves and its interface deforms, a meshfree particle method [23, 24] based on a pressure projection method is applied to solve the incompressible Navier-Stokes

equations in the liquid phase. Here particles means moving grid points that move with the fluid velocity and carry all fluid quantities, like pressure, density along with them. To solve the two-phase flow problem an approach similar to the immersed boundary method [15] is adopted. The computational domain is decomposed into liquid and gas domains. First a fixed grid (regular or irregular) is generated on the entire domain which is used to solve the BGK model. Then a secondary grid consisting of liquid particles approximating the initial liquid phase is generated. These liquid particles overlap the BGK grids. The interface between the two phases is determined by the liquid particles. In the one-dimensional case, it is easily determined by identifying the leftmost and rightmost liquid particles. For the two-dimensional case the interface is determined by identifying the free surface particles of the liquid phase [23]. The BGK grids, which are overlapped by liquid particles are not considered in the solution procedure of the BGK model. These overlapped grids are considered as *non-active* grid points and the rest are *active* grid points.

In a one dimensional case the coupled solutions of the incompressible Navier-Stokes equations and the BGK model are compared with those of the incompressible Navier-Stokes equations and the Boltzmann equation with DSMC methods. The coupling of the incompressible Navier-Stokes and the Boltzmann equation equations are not repeated in this paper, we refer [21] for details. Moreover, a straight forward extension of $1D$ into $2D$ physical space is presented.

The paper is organised as follows. In section 2 we present the mathematical models including the BGK model for the Boltzmann equation and the incompressible Navier-Stokes equations. In subsection 2.3 we present initial, boundary and interface conditions. In subsection 2.5 the procedure to activate and deactivate the BGK grid points is presented. The determination of free surface particles is explained in subsection 2.4. In section 3 the numerical schemes for the BGK model and the incompressible Navier-Stokes equations are presented. In section 4 we present various numerical results in one and two space dimensions. Finally, in section 5 some conclusion and an outlook are presented.

2. Mathematical model. We consider for simulations of the rarefied gas phase the BGK model of the Boltzmann equation and for the liquid phase the incompressible Navier-Stokes equations.

2.1. Rarefied gas phase: The BGK model of the Boltzmann equation.

We consider the BGK model of the Boltzmann equation for rarefied gas dynamics, where the collision term is modeled by a relaxation of the distribution function $f(t, \mathbf{x}, \mathbf{v})$ to the Maxwellian equilibrium distribution. The evolution equation for the distribution function $f(t, \mathbf{x}, \mathbf{v})$ is given by the following initial boundary value problem

$$\frac{\partial f}{\partial t} + \mathbf{v} \cdot \nabla_{\mathbf{x}} f = \frac{1}{\epsilon} (M - f) \quad (2.1)$$

with $f(0, \mathbf{x}, \mathbf{v}) = f_0(\mathbf{x}, \mathbf{v})$, $t \geq 0$, $\mathbf{x} \in \Omega \subset \mathbb{R}^{d_x}$ ($d_x = 1, 2, 3$), $\mathbf{v} \in \mathbb{R}^{d_v}$ ($d_v = 1, 2, 3$) and suitable initial and boundary conditions described in the next section. In this paper, we consider $d_x = 1$ and 2 , that means, one and two physical space dimensions. Component wise we denote the position and the velocity in $2D$ as $\mathbf{x} = (x, y)$ and $\mathbf{v} = (u, v)$.

Here ϵ is the relaxation time and M is the local Maxwellian given by

$$M = \frac{\rho_g}{(2\pi RT_g)^{d_v/2}} \exp\left(-\frac{|\mathbf{v} - \mathbf{u}_g|^2}{2RT_g}\right), \quad (2.2)$$

where the parameters $\rho_g(\mathbf{x}, t) \in \mathbb{R}$, $\mathbf{U}_g(\mathbf{x}, t) \in \mathbb{R}^{d_v}$, $T_g(\mathbf{x}, t) \in \mathbb{R}$ are the density, mean velocity and temperature, respectively of the gas. R is the universal gas constant. The macroscopic quantities $\rho_g, \mathbf{U}_g, T_g$ are computed from f as the moments of f given by

$$(\rho_g, \rho_g \mathbf{U}_g, E_g) = \int_{\mathbb{R}^{d_v}} \psi(\mathbf{v}) f(t, \mathbf{x}, \mathbf{v}) d\mathbf{v}. \quad (2.3)$$

where $\psi(\mathbf{v}) = \left(1, \mathbf{v}, \frac{|\mathbf{v}|^2}{2}\right)$ denotes the vector of collision invariants. E_g is the total energy density which is related to the temperature through the internal energy

$$e_g(t, \mathbf{x}) = \frac{d_v}{2} R T_g, \quad \rho_g e_g = E - \frac{1}{2} \rho_g |\mathbf{U}_g|^2. \quad (2.4)$$

The gas pressure p_g is defined as $p_g = \frac{2}{3} \rho_g e_g$ for a monoatomic ideal gas. For more details we refer to [2, 18]. Moreover, the gas pressure tensor φ_g is defined by

$$\varphi_g = \int_{\mathbb{R}_v^d} (\mathbf{v} - \mathbf{U}_g) \otimes (\mathbf{v} - \mathbf{U}_g) f(t, \mathbf{x}, \mathbf{v}) d\mathbf{v} \quad (2.5)$$

and the gas stress tensor τ_g is defined by

$$\varphi_g = p_g \mathbb{I} - \tau_g. \quad (2.6)$$

The relaxation time $\epsilon = \epsilon(t, \mathbf{x})$ and the mean free path λ are related according to [3]

$$\epsilon = \frac{4\lambda}{\pi \bar{C}}, \quad (2.7)$$

where $\bar{C} = \sqrt{\frac{8RT_g}{\pi}}$ and the mean free path is given by

$$\lambda = \frac{k_b}{\sqrt{2\pi\rho R d^2}},$$

where k_b is the Boltzmann constant and d is the diameter of the gas molecules.

2.2. Liquid phase: Incompressible Navier-Stokes equations. We consider an incompressible flow inside the liquid phase. In the above subsection we have considered the macroscopic quantities of the gas with the index g . For the liquid we denote all quantities with the index l . In this paper we consider a liquid with constant temperature, i. e. no heat exchange between liquid and gas phases is considered. The liquid phase is modelled using the incompressible Navier-Stokes equations given by

$$\nabla \cdot \mathbf{U}_l = 0 \quad (2.8)$$

$$\rho \left(\frac{\partial \mathbf{U}_l}{\partial t} + (\mathbf{U}_l \cdot \nabla) \mathbf{U}_l \right) = -\nabla \cdot \varphi_l, \quad (2.9)$$

where

$$\varphi_l = p_l \mathbb{I} - \tau_l = p_l \mathbb{I} - \mu_l (\nabla \mathbf{U}_l + (\nabla \mathbf{U}_l)^T) \quad (2.10)$$

and μ_l is the dynamic viscosity.

We note that the gravitational force is neglected in this paper.

2.3. Initial and boundary conditions. In this paper we consider one- and two-dimensional computational domains $\Omega \subset \mathbb{R}^{1,2}$ with a boundary Γ . The domain is initially decomposed into the gas domain Ω_g and liquid domain $\Omega_l = \Omega \setminus \Omega_g$, see Figure 2.1.

2.3.1. Initial conditions. In the gas domain Ω_g we solve the BGK model. We assume that initially the gas is in thermal equilibrium, which is prescribed by the local Maxwellian with the parameters $\rho_g(0, \mathbf{x})$, $\mathbf{U}_g(0, \mathbf{x})$ and $T_g(0, \mathbf{x})$. Moreover, in liquid domain Ω_l we solve the incompressible Navier-Stokes equations with the initial values for $\mathbf{U}_l(0, \mathbf{x})$, $p_l(0, \mathbf{x})$.

2.3.2. Boundary conditions for BGK model. We consider cases where the liquid domain always remains inside the gas domain and does not contact with solid walls. Therefore, the boundary Γ always belongs to the gas domain. Moreover, there are interfaces between the liquid and the gas domains, which is denoted by Γ_l and we have to further specify the interface boundary conditions. So, first, we generate the solid boundary points on solid walls. Then, we generate the fixed interior grids for the BGK model. Finally, we generate the liquid particles overlapping the fixed grid points, see right of Figure 2.1, where red grid points are solid wall points, black points are *active* grid points for the gas phase, grey points are *non-active* grid points and blue points are particles for the liquid phase. In section 2.5 the procedure to activate and deactivate grid points is described.

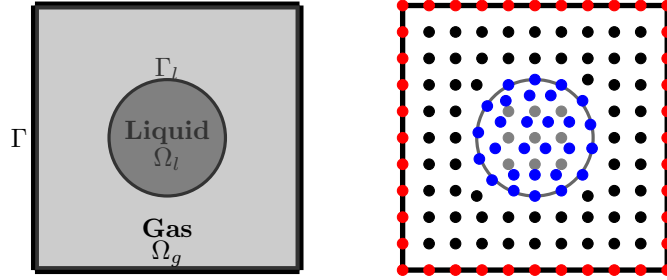


Fig. 2.1: Left: Liquid drop Ω_l with interface boundary Γ_l immersed in the gas. Right: Black circles are active interior gas grid points, red circles are boundary grid points, which are always *active*. The grey grid points are *non-active* gas grid points and the blue points are liquid particles.

On the solid as well as the interface boundaries we apply diffuse reflection boundary conditions with constant temperature $T(0, \mathbf{x})$ and wall velocity \mathbf{U}_B . The boundary particles are sitting on the boundaries and all boundary points having contact with the gas phase are defined as *active* points. Let ρ_B and \mathbf{n} be the density and the unit normal vector of the wall and the free surface of the liquid. The normal vector \mathbf{n} points towards the gas domain.

For $(\mathbf{v} - \mathbf{U}_B) \cdot \mathbf{n} < 0$ we obtain the distribution function on the wall f_B^{n+1} from the evolution equation. For $(\mathbf{v} - \mathbf{U}_B) \cdot \mathbf{n} > 0$ the distribution function is the Maxwellian with parameters ρ_B, T and \mathbf{U}_B , given by

$$M_B^{n+1} = \frac{\rho_B}{(2\pi RT)^{d_v/2}} \exp\left(-\frac{|\mathbf{v} - \mathbf{U}_B|^2}{2RT}\right). \quad (2.11)$$

We note that the density ρ_B is not known and is determined by assuming the net flux across the wall or surface is zero. This means, we have

$$\int_{\mathbb{R}^{d_v}, (\mathbf{v}-\mathbf{U}_B) \cdot \mathbf{n} > 0} [(\mathbf{v}-\mathbf{U}_B) \cdot \mathbf{n}] M_B^{n+1} d\mathbf{v} + \int_{\mathbb{R}^{d_v}, (\mathbf{v}-\mathbf{U}_B) \cdot \mathbf{n} < 0} [(\mathbf{v}-\mathbf{U}_B) \cdot \mathbf{n}] f_B^{n+1} d\mathbf{v} = 0. \quad (2.12)$$

Hence, from (2.11) and (2.12) we obtain

$$\rho_B = - \frac{\int_{\mathbb{R}^{d_v}, (\mathbf{v}-\mathbf{U}_B) \cdot \mathbf{n} < 0} [(\mathbf{v}-\mathbf{U}_B) \cdot \mathbf{n}] f_B^{n+1} d\mathbf{v}}{\int_{\mathbb{R}^{d_v}, (\mathbf{v}-\mathbf{U}_B) \cdot \mathbf{n} > 0} [(\mathbf{v}-\mathbf{U}_B) \cdot \mathbf{n}] \frac{1}{(2\pi RT)^{d_v/2}} \exp\left(-\frac{|\mathbf{v}-\mathbf{U}_B|^2}{2RT}\right) d\mathbf{v}}. \quad (2.13)$$

2.3.3. Interface boundary conditions for liquid phase. We assume that the liquid phase does not interact with the solid boundaries. Thus, we have to prescribe conditions only on the interface boundaries of liquid and gas phase. The interface boundaries are obtained by determining the free surface boundary particles of the liquid phase, see subsection 2.4. These interface particles have to be tracked at every time step. Since we neglected heat exchange between the two phases, we simply prescribe the interface conditions on velocity and stress tensors. Here, we denote again by \mathbf{n} the normal at the interface pointing into the gas domain. First, we assume that the velocity is continuous across the interface, i.e.

$$[\mathbf{U}]_I = 0 \quad (2.14)$$

where $[\cdot]_I$ denotes the jump across the interface I , for example, $[\mathbf{U}]_I = \mathbf{U}_g - \mathbf{U}_l$.

Owing to the kinematic condition at the interface, there is no penetration of particles from one phase to the other. This means that the convective terms for mass and momentum across the interface are zero. Hence, all fluxes with the multiplicative factors \mathbf{U} vanish. Therefore, we have the following jump conditions for the momentum

$$[\varphi \cdot \mathbf{n}]_I = \sigma \kappa \mathbf{n} \quad (2.15)$$

where σ is the surface tension of a liquid and κ is the curvature of the surface. From (2.15) we get the following continuity relations of the normal and tangential stresses

$$p_g = p_l + \mathbf{n} \cdot \boldsymbol{\tau}_g \cdot \mathbf{n} - \mathbf{n} \cdot \boldsymbol{\tau}_l \cdot \mathbf{n} + \sigma \kappa \quad (2.16)$$

$$\mathbf{t} \cdot \boldsymbol{\tau}_l \cdot \mathbf{n} = \mathbf{t} \cdot \boldsymbol{\tau}_g \cdot \mathbf{n}, \quad (2.17)$$

where \mathbf{t} is the tangent vector on the interface. When we solve the incompressible Navier-Stokes equations, we apply the interface boundary conditions (2.14) and (2.15) on the interface particles of the liquid phase.

2.4. Determination of the free surface particles. In this subsection we present a brief description of the strategy how to find the interface between liquid and gas phases. The interface is obtained by finding the free surface particles. In general, we have a set of grid points including the fixed grids for the BGK model and the moving grids for the incompressible Navier-Stokes equations. When we search a neighbor list of grid points or particles for one phase, we exclude the grid points from the other phase. Therefore, when searching for the free surface particles of the liquid phase, we exclude all grid points from the gas phase. For determination of the free surface particles we refer [23] for details. We describe the procedure shortly for the 2D case. We note, that the free surface particles are not known a priori, however it is

important to have a very accurate selection of them, otherwise the whole numerical procedure and application of interface boundary conditions is likely to fail. We say that a particle at the position x_i belongs to the free surface, if we can place a sphere in the neighborhood of the particle such that

- \mathbf{x}_i lies on the surface of the sphere (i.e. it is not the center)
- the radius of the sphere is $r_S = \beta \cdot h$ where h is about 2.5 to 3.5 times the initial spacing and β is a constant, preferably in the range between 0.7 to 1.0.
- no other particle lies inside of the sphere.

We note that this means that interior holes have to be filled with particles before their radius reaches the magnitude of r_S .

The effort of searching surface particles is huge and can take up to 10 percent of the over-all-computation-time. It can be reduced by

- considering only those particles as candidates for being at the free surface at time level t_n , which are in the neighborhood of a free surface particle at time level t_{n-1} (this reduces the number of particles to be checked)
- doing the search for the free surface particles not for each time step.

For the computation of curvature and normal on free surface particles we refer to the works reported in [23].

2.5. Activating/deactivating BGK grid points. We generate the entire domain including boundaries by fixed grids, where we compute the gas phase. In order to simulate the interaction of liquid and gas, we additionally generate the liquid particles approximating liquid domain. The gas grid points and the liquid particles are decoupled. These liquid particles overlap the fixed grid points. For the numerical simulation of the gas phase we have *active* as well as *non-active* grid points. Those grid points in the gas phase which are overlapped by the liquid domain during the motion are defined as *non-active* grid points and the others as *active* grid points. After moving the liquid particles, some of the active grid points will overlap with the liquid particles and are then redefined as *non-active* grid points. In turn, some of the *non-active* grid points will be out of the overlapping zone of the liquid phase and will be reactivated again for the numerical process. During this process we need to update the distribution function $f(t, \mathbf{x}, \mathbf{v})$ on the newly activated grids. This can be obtained from its neighboring *active* grid points using the least squares method. We note that the interface liquid particles are added as *active* for the gas phase.

The process of finding the fixed grid points which are overlapped by the liquid domain is as follows: consider an arbitrary fixed grid point. If this grid point does not have any liquid particle as neighbor, it is a non-overlapping grid point. If the neighbourhood of the fixed grid point contains liquid particles then we apply the sphere-placing procedure described in the previous subsection to the fixed grid point and use it to determine whether the fixed grid point is inside or outside of the liquid domain.

3. Numerical schemes. In this section we present the numerical schemes for the BGK model and the incompressible Navier-Stokes equations. The BGK model is solved by the Semi-Lagrangian scheme suggested in [17], where the authors have used an interpolation scheme based on classical mesh-based method and ghost points have to be added to treat boundary conditions. In this paper, we employ a meshfree interpolation scheme based on the moving least squares method for the reconstruction and adding the ghost points is not necessary. When a drop moves and deforms one has to re-mesh and can be costly and complicated. Therefore, we apply a meshfree interpolation scheme. Moreover, the incompressible Navier-Stokes equations are also solved by a mesh free particle method based on the moving least squares methods.

3.1. Semi-Lagrangian scheme for the BGK model. We consider a constant time step Δt , a uniform mesh in velocity space with mesh size Δv and a, in general, non-uniform mesh with average spacing Δx in physical space. The time discretization is denoted by $t_n = n\Delta t, n = 0, 1, \dots$. In this section, we describe the discretization procedure for two-dimensional physical cases. For the one dimensional cases the second component is just omitted. The space discretization is obtained by filling (regular or irregular) grid points $\mathbf{x}_i = (x_i, y_i) \in \Omega \subset \mathbb{R}^2, i = 1, \dots, N_x$, where N_x is the total number of grid points in physical space. These are the fixed BGK grid points. We note that the N_x grid points include active and in-active interior as well as boundary points. The BGK model is solved only on the active points and the interpolation is also obtained from the active neighboring points only. The interface particles are the free surface particles of the liquid phase, where we apply the boundary conditions on these interface particles for the gas phase. See Figure 2.1 for an illustration. If the interface particles are within the radius of a BGK grid point we add them in the reconstruction process of the distribution function.

Moreover, we consider an even number N_v of velocity grid points in each direction and a uniform velocity grid size Δv in all directions. We assume the distribution function is negligible for $|\mathbf{v}| > \mathbf{v}_{max} = \frac{N_v \Delta v}{2}$. The velocity grid points are denoted by u_j and v_k in x and y directions, respectively, where $u_j = -u_{max} + (j-1)\Delta v, j = 1, \dots, N_v + 1$. Similarly, we define v_k for $k = 1, \dots, N_v + 1$.

Let $f_{jk} = f_{jk}(t, x, y) = f(t, x, y, u_j, v_k)$ and $f_{ijk} = f_{ijk}(t) = f(t, x_i, y_i, u_j, v_k)$. The evolution equation of $f_{jk}(t, x, y)$ along the characteristics between time steps n and $n+1$, i.e., for $t \in [t_n, t_{n+1}]$, is calculated from the Lagrangian form of the discrete-velocity BGK model

$$\frac{df_{jk}}{dt} = \frac{1}{\epsilon}(M_{jk}[f] - f_{jk}) \quad (3.1)$$

$$\frac{dx}{dt} = u_j, \quad (3.2)$$

$$\frac{dy}{dt} = v_k, \quad (3.3)$$

with final conditions

$$(x, y)(t_n) = (\tilde{x}, \tilde{y}), \quad f_{jk}(t_n) = f_{jk}^n(\tilde{x}, \tilde{y}) = \tilde{f}_{jk}^n \quad (3.4)$$

together with appropriate boundary conditions for f_{jk} at boundary points.

Here $M_{jk}[f]$ is still the local Maxwellian having the moments of f_{jk} .

We consider the implicit Euler scheme for the above equations, which reads

$$f_{ijk}^{n+1} = \tilde{f}_{ijk}^n + \frac{\Delta t}{\epsilon}(M_{ijk}^{n+1}[f] - f_{ijk}^{n+1}), \quad (3.5)$$

and

$$x_i^{n+1} = \tilde{x} + v_j \Delta t, \quad y_i^{n+1} = \tilde{y} + v_k \Delta t \quad (3.6)$$

for $j, k = 1 \dots, N_v + 1$ and all active interior points i .

The semi-Lagrangian method now consists of three steps:

(i) First, we determine \tilde{x} and \tilde{y} from the backward characteristics $\tilde{x} = x_i^{n+1} - u_j \Delta t$, $\tilde{y} = y_i^{n+1} - v_k \Delta t$. Then reconstruct the function \tilde{f}_{jk}^n at (\tilde{x}, \tilde{y}) . At t^n all values f_{ijk}^n are known for all active points and boundary points. At (\tilde{x}, \tilde{y}) we have to interpolate

\tilde{f}_{ijk}^n . One can use any interpolation formula. In this paper we use a least squares approximation for the reconstruction, which is presented in subsection 3.4.

(ii) In the second step we obtain M_{ijk}^{n+1} . Since M_i^{n+1} and f_i^{n+1} give the same conservative moments, we multiply the above discrete equation by the discrete collisional invariants $1, u_j, v_k, \frac{1}{2}(u_j^2 + v_k^2)$ and sum over all velocities. We get

$$\begin{aligned}\rho_{i,g}^{n+1} &= \sum_{j=1,k}^{N_v+1} \tilde{f}_{ijk}^n \Delta v^2, \quad (\rho U_{i,g})^{n+1} = \sum_{j,k=1}^{N_v+1} u_j \tilde{f}_{ijk}^n \Delta v^2, \\ (\rho V_{i,g})^{n+1} &= \sum_{j,k=1}^{N_v+1} v_k \tilde{f}_{ijk}^n \Delta v^2, \quad E_{i,g}^{n+1} = \frac{1}{2} \sum_{j,k=1}^{N_v+1} (u_j^2 + v_k^2) \tilde{f}_{ijk}^n \Delta v^2.\end{aligned}\quad (3.7)$$

Once the moments are known, we can compute the Maxwellian at the new time. We note that we write the mean velocity componentwise as $\mathbf{U} = (U, V)$ for both phases.

(iii) Finally, we update the density function by

$$f_{ijk}^{n+1} = \frac{\tau \tilde{f}_{ijk}^n + \Delta t M_{ijk}^{n+1}}{\epsilon + \Delta t}. \quad (3.8)$$

On the solid and interface boundary points we apply the diffuse reflection boundary conditions. Which means, interpolate the distribution function on these boundary points and apply the boundary condition according to (2.11) in the discrete form.

3.2. Projection method for the incompressible Navier-Stokes equations. For the liquid phase we solve the incompressible Navier-Stokes equations (3.9) by a meshfree Lagrangian particle method, therefore, we re-express these equations in the Lagrangian form is given by

$$\begin{aligned}\frac{d\mathbf{x}_l}{dt} &= \mathbf{U}_l \\ \nabla \cdot \mathbf{U}_l &= 0 \\ \frac{d\mathbf{U}_l}{dt} &= -\frac{\nabla p_l}{\rho_l} + \nu_l \nabla^2 \mathbf{U}_l,\end{aligned}\quad (3.9)$$

where ν_l is the kinematic viscosity. The system of equations (3.9) is solved using Chorin's projection method [4]. This method consists of two fractional steps and is of first order accuracy in time. In the first step the new particle positions are computed explicetely and intermediate velocities \mathbf{U}_l^* are computed implicitly by

$$\mathbf{x}_l^{n+1} = \mathbf{x}_l^n + \Delta t \mathbf{U}_l^n, \quad (3.10)$$

$$\mathbf{U}_l^* = \mathbf{U}_l^n + \Delta t \nu_l \Delta \mathbf{U}_l^*. \quad (3.11)$$

Then, in the second step we correct \mathbf{U}_l^* considering

$$\mathbf{U}_l^{n+1} = \mathbf{U}_l^* - \frac{\Delta t}{\rho_l} \nabla p_l^{n+1} \quad (3.12)$$

together with the incompressibility constraint

$$\nabla \cdot \mathbf{U}_l^{n+1} = 0. \quad (3.13)$$

By taking the divergence of equation (3.12) and by making use of (3.13) we finally obtain the pressure Poisson equation

$$\Delta p_l^{n+1} = \frac{\rho_l}{\Delta t} \nabla \cdot \mathbf{U}_l^*. \quad (3.14)$$

We note that the particle positions change only in the first step. The intermediate velocity \mathbf{U}_l^* is then obtained at these new particle positions. In the discretised equations we have to compute the first and second spatial derivatives. These derivatives are computed using again the least squares method described in subsection 3.4. Furthermore, the intermediate velocity equation (3.11) and the pressure Poisson equation (3.14) are elliptic equations of the type

$$A\psi + B\Delta\psi = f, \quad (3.15)$$

where A, B, f are given constants. For the vector equation (3.11), for example, the x -component of the velocity has coefficients $A = 1, B = -\Delta t \nu_l$ and the source term has $f = U_l^n$ and for the pressure Poisson equation (3.14) the coefficients and the source term are $A = 0, B = 1$ and $f = \frac{\rho_l}{\Delta t} \nabla \cdot \mathbf{U}_l^*$, respectively. We have to solve two elliptic equations for velocity and one for pressure at every time step. All three elliptic equations are solved by a meshfree particle method presented in subsection 3.5.

For the pressure Poisson equation we apply the Dirichlet boundary condition (2.16) on the free surface (or interface) points. The interface condition (2.17) is applied while computing the intermediate velocity by adding this condition as additional constraint and is given by

$$a_1 \frac{\partial U_l}{\partial x} + a_2 \frac{\partial U_l}{\partial y} + a_3 \frac{\partial V_l}{\partial x} + a_4 \frac{\partial V_l}{\partial y} = \mathbf{t} \cdot \boldsymbol{\tau}_g \cdot \mathbf{n}, \quad (3.16)$$

where $a_1 = 2\mu_l t_1 n_1, a_2 = a_3 = \mu_l(t_1 n_2 + t_2 n_1), a_4 = 2\mu_l t_2 n_2$, where $\mathbf{n} = (n_1, n_2)$ and $\mathbf{t} = (t_1, t_2)$, see [21, 23] for details.

- 3.3. Coupling Algorithm.** (i) Generate BGK grid points in the entire domain and generate liquid particles overlapping the BGK points.
(ii) Initialize the distribution function outside the liquid domain according to a Maxwellian with the given initial parameters and prescribe the initial conditions for the liquid particles.
(iii) Determine the free surface particles for the liquid phase.
(iv) Solve the BGK model with the gas-liquid interface taking the role of a moving interface.
(v) Compute the moments on the BGK grids and interface particles.
(vi) Solve the incompressible Navier-Stokes equations.
(vii) Add or remove liquid particles, if necessary.
(viii) Goto (iii) and repeat until the final time is reached.

3.4. Interpolation and approximation of derivatives. We describe the general approximation procedure in a two-dimensional spatial domain. $\Omega \in \mathbb{R}^2$. Approximate Ω by particles or grid points with position $(x_i, y_i), i = 1, \dots, N$, whose distribution can be irregular, see Figure 3.1. As already mentioned the grid points for the gas phase are fixed and the grid points for the liquid phase move with their velocity. We store both type of grids in an array but assign separate flags for each phase. In the neighbor list for a particle of one of the phases, we exclude the points belonging to the other phase to determine the corresponding derivatives.

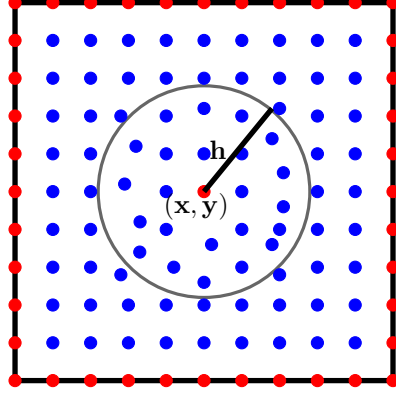


Fig. 3.1: Approximation of a domain by grid points or particles

Let $\psi(x, y)$ be a scalar function and $\psi_i = \psi(x_i, y_i)$ be its discrete values for $i = 1, \dots, N$.

We consider the problem to interpolate or approximate the spatial derivatives at an arbitrary point $(x, y) \in \Omega$, in terms of the values of a set of its values at neighboring points. We note that the point (x, y) is not necessarily one of the grid points. In order to restrict the number of neighboring points we define a weight function $w = w(x_i - x, y_i - y, h)$ with small compact support of size h . The value of h has to be chosen such that we have at least a minimum number of particles, for example, in $2D$, we need at least 6 neighboring points if we want to obtain second order approximations. In practice we define h as 2.5 to 3 times the initial spacing of particles, keeping in mind that this is a user defined factor. The weight function can be quite arbitrary. In our case we consider a Gaussian weight function defined as

$$w_i = w(r_i; h) = \begin{cases} \exp(-\alpha \frac{r_i^2}{h^2}), & \text{if } \frac{r}{h} \leq 1 \\ 0, & \text{else} \end{cases} \quad (3.17)$$

where $r_i = \sqrt{(x_i - x)^2 + (y_i - y)^2}$ and α is equal to 6.25. In general, the value of α has to be chosen according to the choice of h such that the approximation of spatial derivatives is accurate. In this paper, we have chosen h is equal to 3 times the initial spacing of particles, so this choice of α gives an accurate approximation of spatial derivatives. Let $P(x, y, h) = \{(x_j, y_j) : j = 1, 2, \dots, m\}$ be the set of m neighboring points of (x, y) in a circle of radius h . Consider m Taylor expansions of $\psi(x_j, y_j)$ around (x, y)

$$\begin{aligned} \psi(x_j, y_j) = \psi(x, y) + \frac{\partial \psi}{\partial x}(x_j - x) + \frac{\partial \psi}{\partial y}(y_j - y) + \frac{1}{2} \frac{\partial^2 \psi}{\partial x^2}(x_j - x)^2 + \\ \frac{\partial^2 \psi}{\partial x \partial y}(x_j - x)(y_j - y) + \frac{1}{2} \frac{\partial^2 \psi}{\partial y^2}(y_j - y)^2 + e_j \end{aligned} \quad (3.18)$$

for $j = 1, \dots, m$, where e_j is the residual error. Assume that $u(x, y)$ approximates its nearest neighbor value, denoted by ψ_{min} . Subtracting the value ψ_{min} on both side of (3.18) and denote the coefficients

$$a_1 = \psi(x, y) - \psi_{min}, \quad a_2 = \frac{\partial \psi}{\partial x}, \quad a_3 = \frac{\partial \psi}{\partial y},$$

$$a_4 = \frac{\partial^2 \psi}{\partial x^2}, \quad a_5 = \frac{\partial^2 \psi}{\partial x \partial y}, \quad a_6 = \frac{\partial^2 \psi}{\partial y^2}.$$

We have six unknowns $a_i, i = 1, \dots, 6$. Now we have to solve m equations for six unknowns. For $m > 6$ this system is overdetermined and can be written in matrix form as

$$\mathbf{e} = -(\mathbf{M}\mathbf{a} - \mathbf{b}), \quad (3.19)$$

where

$$\mathbf{M} = \begin{pmatrix} dx_1 & dy_1 & \frac{1}{2}dx_1^2 & dx_1dy_1 & \frac{1}{2}dy_1^2 \\ \vdots & \vdots & \vdots & \vdots & \vdots \\ dx_m & dy_m & \frac{1}{2}dx_m^2 & dx_mdy_m & \frac{1}{2}dy_m^2 \end{pmatrix}, \quad (3.20)$$

$\mathbf{a} = (a_1, a_2, \dots, a_6)^T$, $\mathbf{b} = (\psi_1 - \psi_{min}, \dots, \psi_m - \psi_{min})^T$, $\mathbf{e} = (e_1, \dots, e_m)^T$ and $dx_j = x_j - x$, $dy_j = y_j - y$.

The unknowns a_i are computed by minimizing a weighted error over the neighboring points. Thus, we have to minimize the following quadratic form

$$J = \sum_{i=1}^m w_i e_i^2 = (\mathbf{M}\mathbf{a} - \mathbf{b})^T \mathbf{W} (\mathbf{M}\mathbf{a} - \mathbf{b}), \quad (3.21)$$

where

$$\mathbf{W} = \begin{pmatrix} w_1 & 0 & \dots & 0 \\ \vdots & \vdots & \dots & \vdots \\ 0 & 0 & \dots & w_m \end{pmatrix}.$$

The minimization of J with respect to a formally yields (if $M^T W M$ is nonsingular)

$$\mathbf{a} = (\mathbf{M}^T \mathbf{W} \mathbf{M})^{-1} (\mathbf{M}^T \mathbf{W}) \mathbf{b} := (r_1, \dots, r_m)^T. \quad (3.22)$$

Equating the first coefficient of (3.22) yields

$$\psi - \psi_{min} = r_1 \quad \implies \quad \psi = \psi_{min} + r_1 \quad (3.23)$$

which is the interpolated value at (x, y) . Similarly, equating other coefficients of (3.22) give the spatial derivatives of ψ at (x, y) .

3.5. Solving the Poisson equation. We consider the Poisson equation

$$A\psi + B\Delta\psi = f, \quad (3.24)$$

where $A, B \in \mathbb{R}$ are given constant and the source term f is also given. The equation is solved with Dirichlet or Neumann boundary conditions

$$\psi = g \quad \text{or} \quad \frac{\partial \psi}{\partial n} = g. \quad (3.25)$$

In fact, we can substitute the partial differential operators appearing in equation (3.24) by the components of a from equation (3.22). This approach was first proposed in [12].

In the following we describe an improved meshfree particle method for this problem, see [10] for details. This method can easily handle Neumann boundary condition and has a second-order convergence.

We again consider an arbitrary particle position (x, y) having m neighbors, as in subsection (3.4). We reconsider the m Taylor expansions of equation (3.18). We add the constraint that at particle position (x, y) the partial differential equation (3.24) should be satisfied. If the point (x, y) lies on the boundary, also the boundary conditions (3.25) need to be satisfied. Therefore, we add the equations (3.24) and (3.25) to these m equations (3.18). Equations (3.24) and (3.25) are re-expressed as

$$A\psi + B(a_4 + a_6) = f \quad (3.26)$$

$$\psi = g \text{ or } n_1 a_2 + n_2 a_3 = g, \quad (3.27)$$

Here also we have six unknowns $a_i, i = 1, \dots, 6$. Note that, we have $a_1 = \psi$ in this case. For the interior particles equation (3.26) is added as a constraint, and for boundary particles with Dirichlet or Neumann boundary conditions equation (3.27) is added as another constraint. We have 6 unknowns and there are $m + 1$ equations for interior particles and $m + 2$ equations for the boundary particles. We choose the radius h such that we have always more than 6 neighbors, therefore the system of equations is overdetermined with respect to the unknowns a_i . The system of equations can be written in the following matrix form, where the matrix M differs from (3.20) and is given by

$$M = \begin{pmatrix} 1 & dx_1 & dy_1 & \frac{1}{2}dx_1^2 & dx_1dy_1 & \frac{1}{2}dy_1^2 \\ \vdots & \vdots & \vdots & \vdots & \vdots & \vdots \\ 1 & dx_m & dy_m & \frac{1}{2}dx_m^2 & dx_mdy_m & \frac{1}{2}dy_m^2 \\ A & 0 & 0 & B & 0 & B \\ 0 & n_1 & n_2 & 0 & 0 & 0 \end{pmatrix}, \quad (3.28)$$

with the vectors given by

$$\mathbf{a} = (a_1, \dots, a_6)^T, \mathbf{b} = (\psi_1, \dots, \psi_m, f, g)^T, \mathbf{e} = (e_1, \dots, e_m, e_{m+1}, e_{m+2})^T$$

and $W = \text{diag}(w_1, \dots, w_m, 1, 1)$. For the Dirichlet boundary particles, we directly prescribe the boundary conditions. Similarly, the unknowns a_i are computed by minimizing a weighted error function and obtained in the form (3.22). In (3.22) the vector $(M^T W)\mathbf{b}$ is explicitly given by

$$(M^T W)\mathbf{b} = \begin{pmatrix} \sum_{j=1}^m w_j \psi_j + Af, \sum_{j=1}^m w_j dx_j \psi_j + n_1 g, \\ \sum_{j=1}^m w_j dy_j \psi_j + n_2 g, \frac{1}{2} \sum_{j=1}^m w_j dx_j^2 \psi_j + Bf, \\ \sum_{j=1}^m w_j dx_j dy_j \psi_j, \frac{1}{2} \sum_{j=1}^m w_j dy_j^2 \psi_j + Bf \end{pmatrix}^T. \quad (3.29)$$

Equating the first components on both sides of equation (3.22), we get

$$\begin{aligned} \psi = & Q_1 \left(\sum_{j=1}^m w_j \psi_j A f \right) + Q_2 \left(\sum_{j=1}^m w_j dx_j \psi_j + n_1 g \right) + \\ & Q_3 \left(\sum_{j=1}^m w_j dy_j \psi_j + n_2 g \right) + Q_4 \left(\frac{1}{2} \sum_{j=1}^m w_j dx_j^2 \psi_j + B f \right) + \\ & Q_5 \left(\sum_{j=1}^m w_j dx_j dy_j \psi_j \right) + Q_6 \left(\frac{1}{2} \sum_{j=1}^m w_j dy_j^2 \psi_j + B f \right), \end{aligned} \quad (3.30)$$

where Q_1, Q_2, \dots, Q_6 are the components of the first row of the matrix $(M^T W M)^{-1}$. Rearranging the terms, we have

$$\begin{aligned} \psi - \sum_{j=1}^m w_j \left(Q_1 + Q_2 dx_j + Q_3 dy_j + Q_4 \frac{dx_j^2}{2} + Q_5 dx_j dy_j + Q_6 \frac{dy_j^2}{2} \right) \psi_j = \\ A Q_1 + B (Q_4 + Q_6) f + (Q_2 n_1 + Q_3 n_2) g. \end{aligned} \quad (3.31)$$

Writing equation (3.31) for all particles $\mathbf{x}_i, i = 1, \dots, N$ gives the following sparse linear system of equations for the unknowns $\psi_i, i = 1, \dots, N$

$$\begin{aligned} \psi_i - \sum_{j=1}^{m(i)} w_{i_j} \left(Q_1 + Q_2 dx_{i_j} + Q_3 dy_{i_j} + Q_4 \frac{dx_{i_j}^2}{2} + Q_5 dx_{i_j} dy_{i_j} + Q_6 \frac{dy_{i_j}^2}{2} \right) \psi_{i_j} = \\ A Q_1 + B (Q_4 + Q_6) f_i + (Q_2 n_1 + Q_3 n_2) g_i. \end{aligned} \quad (3.32)$$

In matrix form we have

$$L \Psi = \mathbf{R}, \quad (3.33)$$

where \mathbf{R} is the right-hand side vector, Ψ is the unknown vector and L is the sparse matrix having non-zero entries only for neighboring particles.

The sparse system (3.33) can be solved by some iterative method. In this paper we apply the method of Gauss-Seidel. In the projection scheme it is also necessary to prescribe initial values for the velocities and pressure at time $t = 0$. For example, we can prescribe a vanishing velocities and pressure initially. Then, in the time iteration the initial values of the velocities and pressure for time step $n + 1$ are taken as the values from time step n . Usually, solving these elliptic equations will require more iterations in the first few time steps. After a certain number of time steps, the values of velocities and pressure at the old time step are close to those of new time step, so the number of iterations required gets reduced.

The iteration process is stopped if the relative error satisfies

$$\frac{\sum_{i=1}^N |\psi_i^{\tau+1} - \psi_i^{(\tau)}|}{\sum_{i=1}^N |\psi_i^{(\tau+1)}|} < \tilde{\epsilon}, \quad (3.34)$$

where $\tau = 0, 1, 2, \dots$, and the approximation to the solution is defined by $\psi(x_i) := \psi^{(\tau+1)}(x_i), i = 1, \dots, N$. The parameter $\tilde{\epsilon}$ is a small positive constant and can be defined by the user. The required number of iterations depends on the values of $\tilde{\epsilon}$ and h .

4. Numerical results. We consider one and two dimensional physical spaces, where a liquid droplet remains completely inside the gas domain and does not touch the solid boundaries. In 1D, we compare the simulations results of the BGK-Navier-Stokes equations with those of the Boltzmann-Navier-Stokes equations, where the Boltzmann equation is solved by a DSMC method [1, 13]. For details of the coupling of Boltzmann and Navier-Stokes equations for moving droplets, we refer to [21]. To compare the solutions with those of the full Boltzmann equation in 1D we consider a three dimensional velocity space for the BGK model. The reduction technique suggested in [5] is applied and the three dimensional velocity space is reduced to a one dimensional velocity space. In the case of a two dimensional physical space, no comparison is made with other methods and a two dimensional velocity space is considered. All the test cases are given in dimensionless form but can be interpreted in SI-unit. For the gas phase we have considered an Argon gas with diameter $d = 0.368 \cdot 10^{-9}$, Boltzmann constant $k_b = 1.3806 \cdot 10^{-23}$ and universal gas constant $R = 208$. For the BGK discretization we have used $N_v = 30$ and $|v_{max}| = 1200$.

4.1. One dimensional droplet driven by a shock in the gas phase. We first consider the interval $\Omega = [0, 1 \cdot 10^{-6}]$. Initially, a liquid droplet occupies the domain $\Omega_l = [4 \cdot 10^{-7}, 6 \cdot 10^{-7}]$, while the gas occupies the rest of the domain. Since in the semi-Lagrangian scheme the grid points are fixed, so a total number of 200 fixed grids are generated for simulations of the gas phase in Ω and 40 moving grid points or particles are generated for the liquid phase overlapping the fixed grid points. The liquid drop and the gas are initially at rest. A shock wave is generated at $x = 2 \cdot 10^{-7}$ with the $\rho_g(0, x) = 1, U_g(0, x) = 0$ and $T(0, x) = 300$. On the right of $x = 2 \times 10^{-7}$ the three initial states are considered which are given by $\rho_g(0, x), U_g(0, x) = 0$ and $T(0, x) = 300$, where $\rho_g(0, x) = 0.25, 0.5$ and 0.8 . The gas is in thermal equilibrium with this initial states. The initial pressure of the gas is computed from the equation of state. The liquid density $\rho_l = 10$ is considered and the initial pressure of the liquid is equal to the one of the gas, see Figure 4.1.

For the DSMC simulations coupled with the incompressible Navier Stokes equations we have used same number of grid points like in the case of the BGK model and the incompressible Navier-Stokes equations. The DSMC results for the Boltzmann equation has inherent fluctuations, therefore, a rather large number of initial gas molecules equal to 20000 per cell is generated. A constant time step $\Delta t = 4 \times 10^{-12}$ is used for both types of equations. Since the incompressible Navier-Stokes equations are solved implicitly, a larger time step can be applied for the liquid phase. For the preseten considerations an equal time step is used for the sake of simplicity.

We note that a similar test case has been studied in [9] for a unit interval, where a inviscid flow has been considered for the gas phase and in [21] where the full Boltzmann equation is solved with the DSMC method for the rarefied gas and the same meshfree method as described above has been used for the incompressible Navier-Stokes equations.

Here the interface points of the liquid drop are x_L and x_R , which are the leftmost and rightmost points belonging to the liquid domain. Those grids point which lie inside $[x_L, x_R]$ are *non-active* and those lying outside this interval are *active* grid points.

In the one dimensional case the divergence free constraint cancels the viscous force and the projection scheme becomes straightfoward. Hence the intermediate velocity

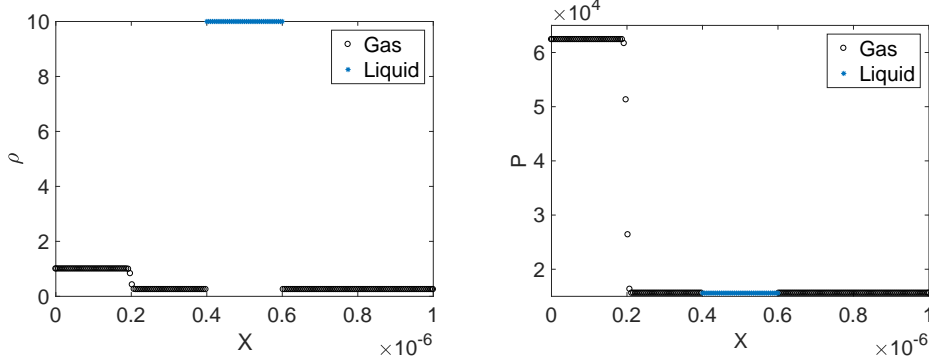


Fig. 4.1: Initial density and pressure of gas and liquid drop for a density ratio 1 : 0.25 for the regions initially left and right of the shock.

remains constant $U_l^* = U_l^n$ and the pressure Poisson equation is given by

$$\frac{\partial^2 p_l^{n+1}}{\partial x^2} = 0 \quad (4.1)$$

with the Dirichlet boundary conditions p_L and p_R at the interface x_L and x_R , respectively. The pressure values p_L and p_R are approximated from the gas phase. Hence, the pressure at every liquid particle with position x is given explicitly by

$$p_l^{n+1}(x) = \frac{p_R^{n+1} - p_L^{n+1}}{x_R^{n+1} - x_L^{n+1}} x^{n+1} + \frac{p_R^{n+1} x_L^{n+1} - p_L^{n+1} x_R^{n+1}}{x_L^{n+1} - x_R^{n+1}}. \quad (4.2)$$

We note that we first move particles and approximate the computed velocity from the gas phase at the interface. Therefore, all quantities on the right hand side of (4.2) are at time level $(n+1)$. The new velocities are given by

$$U_l^{n+1}(x) = U_l^n(x) - \frac{\Delta t}{\rho_l} \left(\frac{p_R^{n+1} - p_L^{n+1}}{x_R^{n+1} - x_L^{n+1}} \right). \quad (4.3)$$

Since the pressure is linear, the velocities are equal for all liquid particles. In this case also the interface conditions are simple. The divergence free constraint implies a vanishing τ_l and we obtain directly the continuity of the velocity and the continuity of normal stress since the interface curvature vanishes.

4.1.1. Case I: Initial density ratio 1 : 0.25. In the first case, we consider an initial density ratio of factor in the regions left and right of the shock discontinuity, see Figure 4.1. In this case the initial mean free path on $[0, 2 \cdot 10^{-7}]$ is equal to $1.103 \cdot 10^{-7}$, which corresponds to the relaxation time $\epsilon = 3.523 \times 10^{-10}$. The corresponding Knudsen number based on a characteristic length given by the size of the droplet is equal to 0.55. The initial mean free path, relaxation time as well as the Knudsen number on the right of the domain are 4 times larger. We observe that the shock hits the drop and starts to push towards the right side. When the drop becomes closer to the right wall, the pressure starts increasing and becomes larger on the right side of the drop. Then the velocity decreases and becomes negative after some time and the drop moves towards the left side of the domain. The drop oscillates and finally

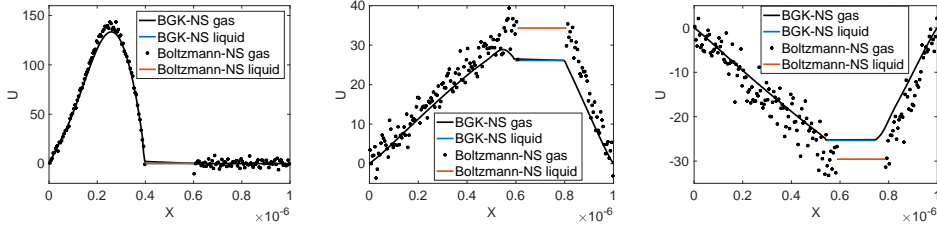


Fig. 4.2: Case I: Velocity of gas and liquid at times $t = 4 \cdot 10^{-10}, 8 \cdot 10^{-9}$ and $1.6 \cdot 10^{-8}$ for the initial density ratio 1 : 0.25.

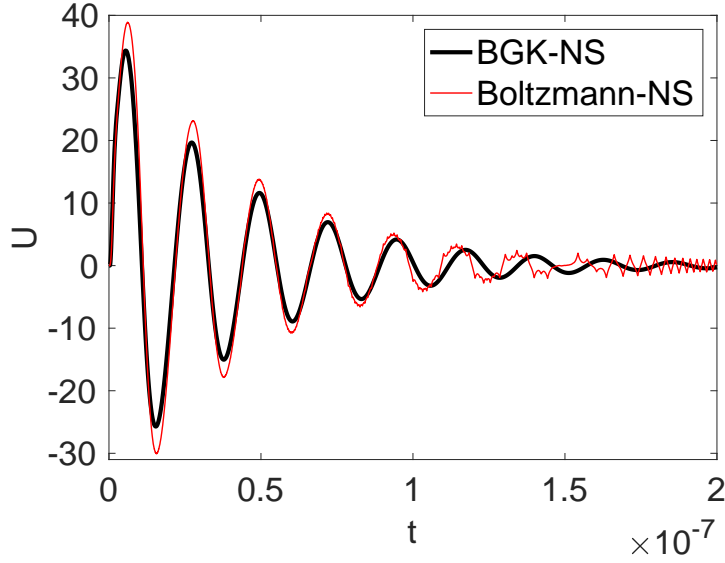


Fig. 4.3: Case I: Velocity of the liquid drop vs time for the density ratio 1 : 0.25.

reaches an equilibrium state with zero velocity. We have plotted the velocity of the gas and liquid phases obtained from the the BGK-Navier-Stokes equations together with the full Boltzmann-Navier-Stokes equations. In Figure 4.2 we have plotted the velocity of the gas and liquid phases at times $t = 4 \cdot 10^{-10}, 8 \cdot 10^{-9}$ and $1.6 \cdot 10^{-8}$. The DSMC solutions oscillates around the BGK solutions. We observe that the drop oscillates back and forth. The pressure difference on the left and right becomes smaller and the velocity of the drop also becomes smaller and smaller. Finally the pressure difference on both sides of the drop become almost equal and the drop stops moving. In Figure 4.3 we have plotted the velocity of the droplet against the time up to the final time $t = 2 \cdot 10^{-7}$. We observe that the coupled solution of the Navier-Stokes and the Boltzmann equations agree very well during the time development.

4.1.2. Case II: Initial density ratio 1 : 0.5. Here the initial density in the region left of the shock is only twice as large as in the region right of the shock. Compared to case I, the initial shock is smaller and the relaxation time and the

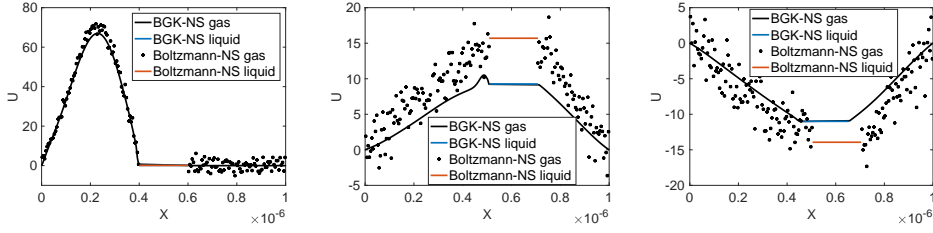


Fig. 4.4: Case II: Velocity of gas and liquid drop at times $t = 4 \cdot 10^{-10}, 8 \cdot 10^{-9}$ and $1.6 \cdot 10^{-8}$ for the initial density ratio 1 : 0.5.

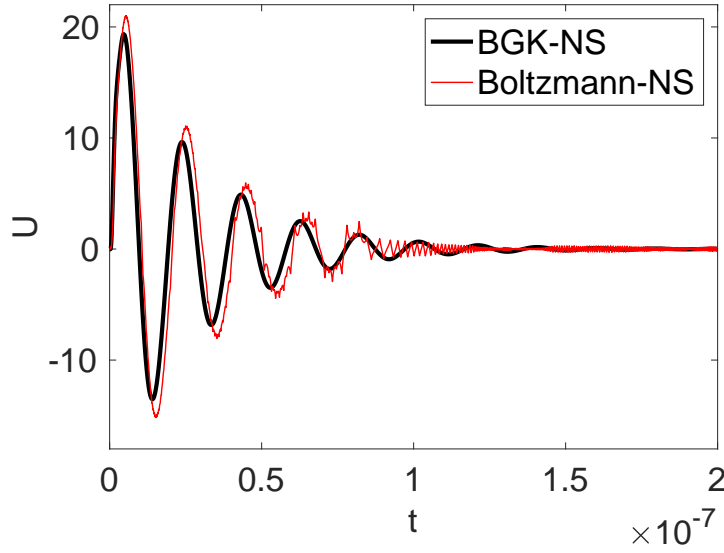


Fig. 4.5: Case II: Velocity of the liquid drop vs time for the density ratio 1 : 0.5.

Knudsen number in the region right of the shock is only twice as large as in the region left of the shock. This gives a smaller initial pressure difference, which yields a smaller force to push the droplet. The mean velocity is also reduced, see Figure 4.4. Here the DSMC results are dominated by the fluctuations, therefore, the discrepancy between the solutions of the BGK-Navier-Stokes equations and the Boltzmann-Navier-Stokes equations increases in the gas phase. However, the behaviour of the droplet velocity is similar like in Case I, see Figure 4.5. In the present case the frequency of oscillations of the droplet is less and the droplet reaches the equilibrium state much earlier than in the previous case.

However, still the velocity of drop with respect to time obtained from both coupled schemes are very close to each other.

4.1.3. Case III: Initial density ratio 1 : 0.8. In the third case we have considered a much smaller initial density or pressure difference between the regions left and right of the shock. The mean flow quantities obtained from the DSMC simulations

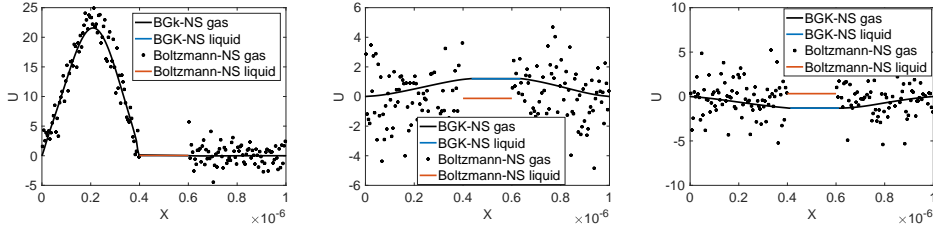


Fig. 4.6: Case III: Velocity of gas and liquid at times $t = 4 \cdot 10^{-10}$, $8 \cdot 10^{-9}$ and $1.6 \cdot 10^{-8}$ for the initial density ratio 1 : 0.8.

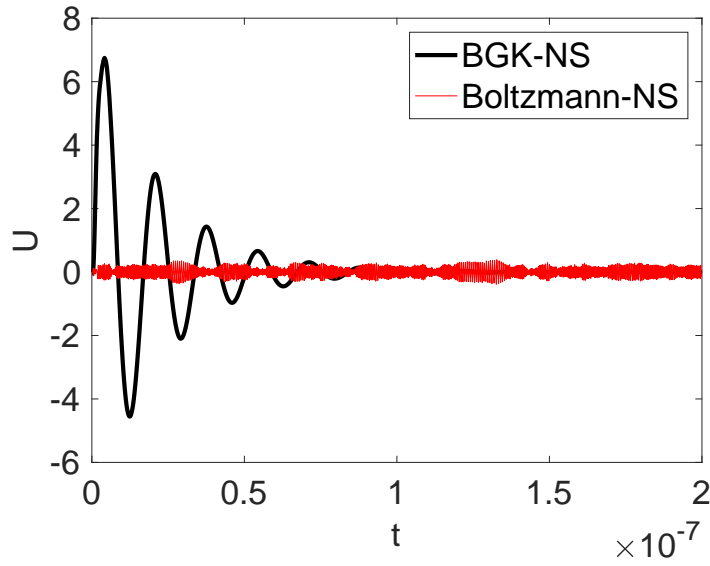


Fig. 4.7: Case III: Velocity of the liquid drop vs time for the density ratio 1 : 0.8.

are completely dominated by the statistical fluctuations, see Figure 4.6 . The drop velocity is almost zero until the final simulation time, see Figure 4.7.

On the other hand, the BGK simulations show an oscillation around the initial zero velocity as in the previous cases. The time until the droplet reaches its final equilibrium position is further reduced compared to Case II.

From all these three cases, we can conclude that for slow flows, classical DSMC simulations are not suitable due to the large statistical fluctuations inherent in these methods. On the contrary, the deterministic method for the BGK model presented here can predict the expected results accurately. We note that Monte Carlo method with noise reduction, see, for example, [8] might be another way to deal with this problem. .

4.2. The two dimensional case.

4.2.1. Movement of droplet in a shock wave. This is the extension of the previous 1D investigations case to two dimensional physical space. A micron size

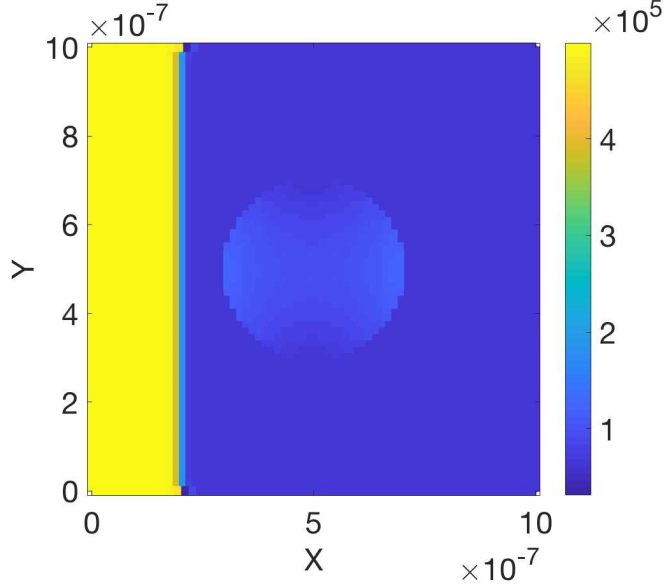


Fig. 4.8: Initial position of droplet and initial pressure.

square is considered as a computational domain. Initially a circular liquid drop of radius $2 \cdot 10^{-7}$ is generated at the center of the square. The initial temperature is 300. A larger density 1 is generated on $x < 2 \cdot 10^{-7}$ and a 4 times lower density is generated on the rest of the domain. The pressure is obtained from the equation of state. In Figure 4.8 we have plotted the initial state of the pressure. The other parameters are chosen as in the one dimensional cases. The time step is chosen as $\Delta t = 2 \cdot 10^{-12}$ for all simulations. The initial pressure of the liquid is equal to the the initial pressure of the gas in the surrounding. Initially the gas and the liquid drop are in rest and the gas is in thermal equilibrium with the initial state. The constant dynamic viscosity of the liquid is $\mu = 2 \cdot 10^{-5}$ considered. The surface coefficient $\sigma = 1 \cdot 10^{-4}$. Since the radius of curvature is of the order of 10^{-7} , the surface tension force is still of the order of 10^3 . In order to observe deformations we have considered liquid densities equal to 2 and 10. The velocity of all walls are zero. Diffuse reflection boundary conditions are applied on all boundaries and on the surface of the liquid drop.

When the membrane is removed, the shock travels to the right and hits the liquid and the liquid starts to move to the right wall. Similar as in the one dimensional case, the drop oscillates. In Figure 4.9 we have plotted only the liquid particles at different times. One observes a slightly stronger deformation of the lighter liquid drop compared to the heavier drop as expected. In Figures 4.10 and 4.11 we have plotted the velocity fields and the pressure at the same time levels.

4.2.2. Movement of droplet in a driven cavity. In the final test case we have considered a liquid drop in the center of a square of micron size as in the previous case. The size of the liquid drop is the same as before. All gas and liquid parameters and the initial states are same as above. The density of the liquid is again given by the values 2 and 10. The upper wall moves with a constant velocity in positive x direction. All other walls have zero velocity. Diffuse reflection boundary conditions

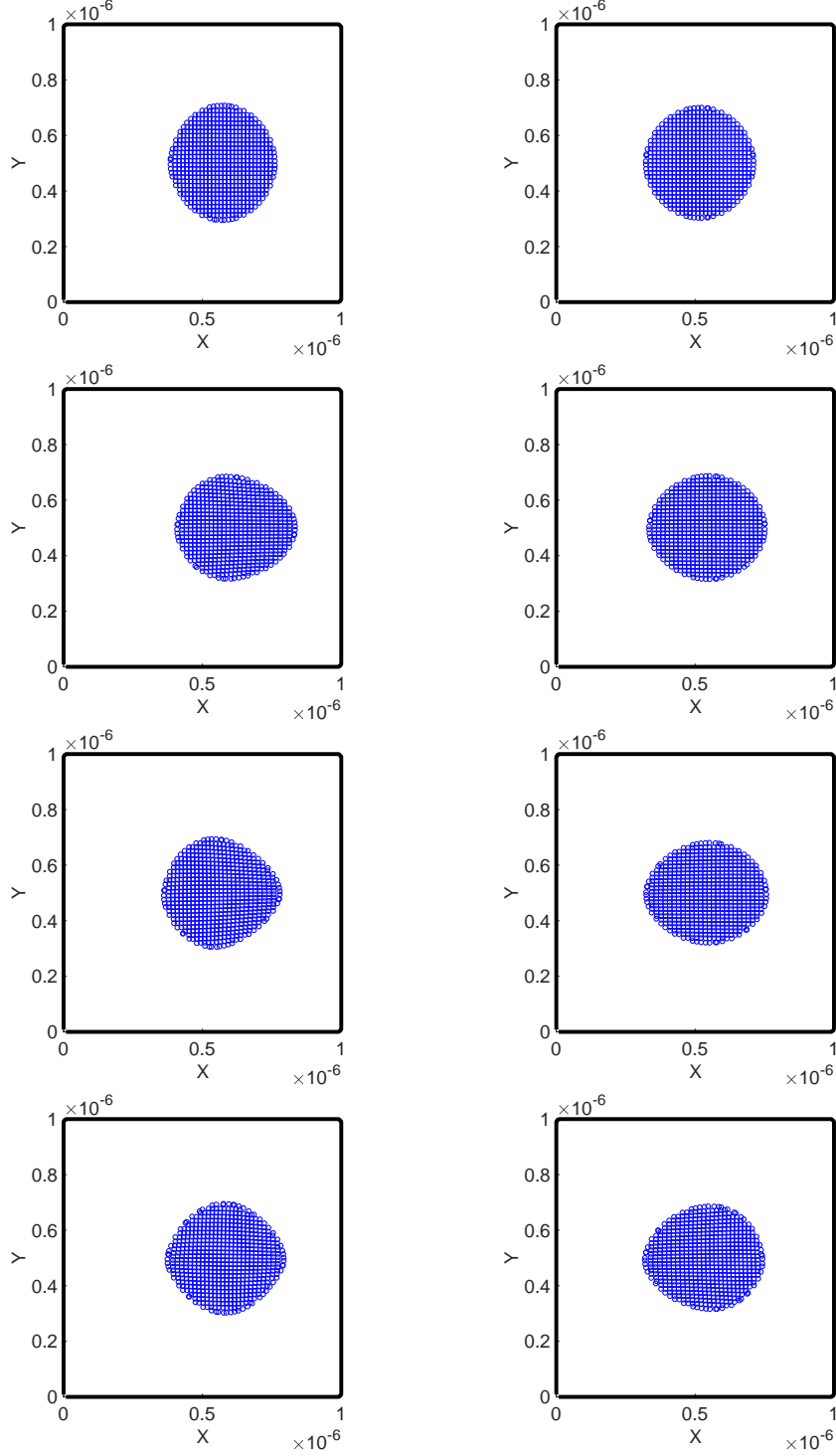


Fig. 4.9: The positions of the droplet at time $t = 2 \cdot 10^{-9}$ (first row), $t = 4 \cdot 10^{-9}$ (second row), $t = 6 \cdot 10^{-9}$ (third row) and $t = 1.4 \cdot 10^{-8}$ (fourth row). Left column: $\rho_l = 2$. Right column: $\rho_l = 10$.

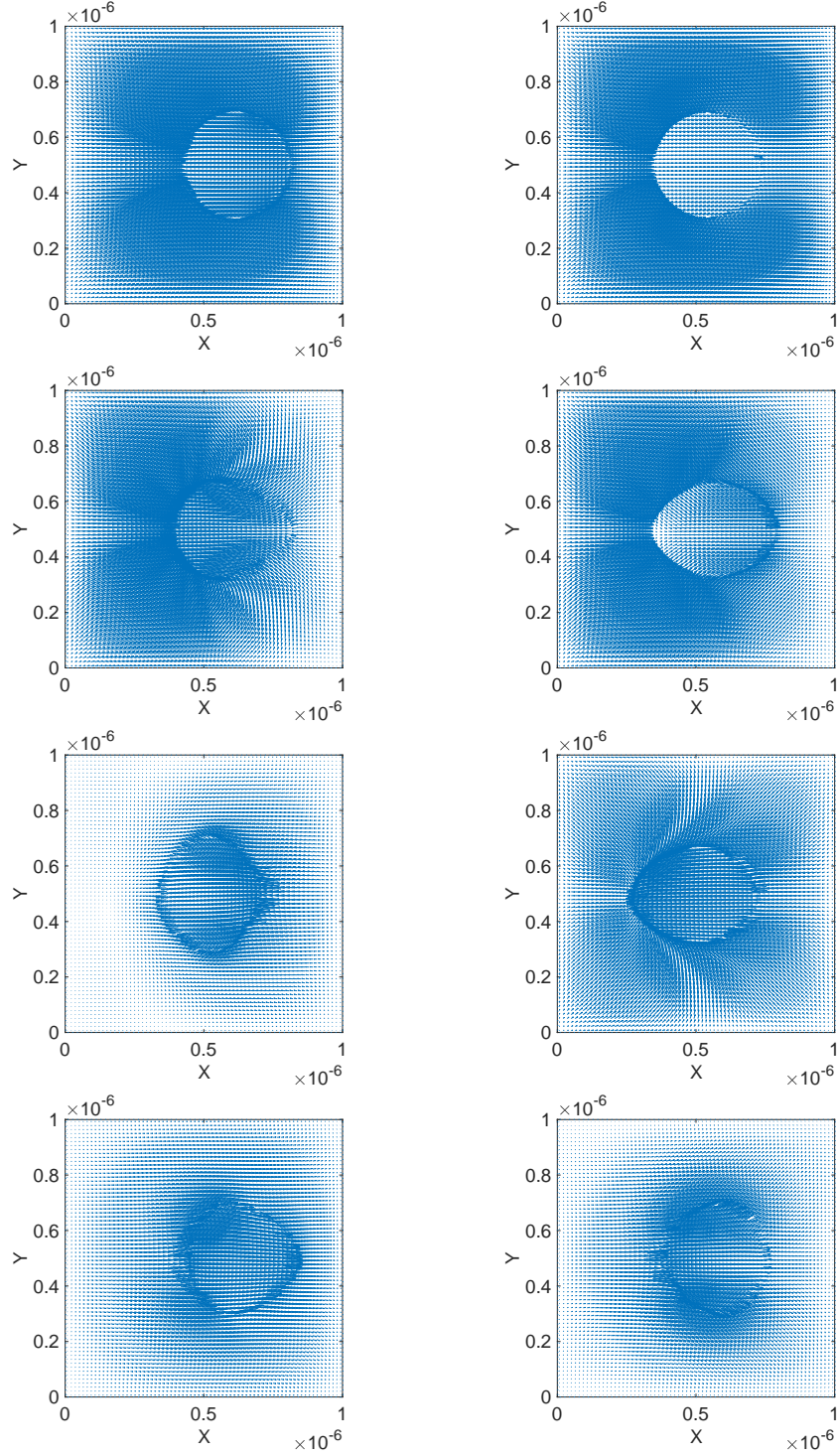


Fig. 4.10: Velocity fields of gas and liquid at time $t = 2 \cdot 10^{-9}$ (first row), $t = 4 \cdot 10^{-9}$ (second row), $t = 6 \cdot 10^{-9}$ (third row) and $t = 1.4 \cdot 10^{-8}$ (fourth row). Left column: $\rho_l = 2$. Right column: $\rho_l = 10$.

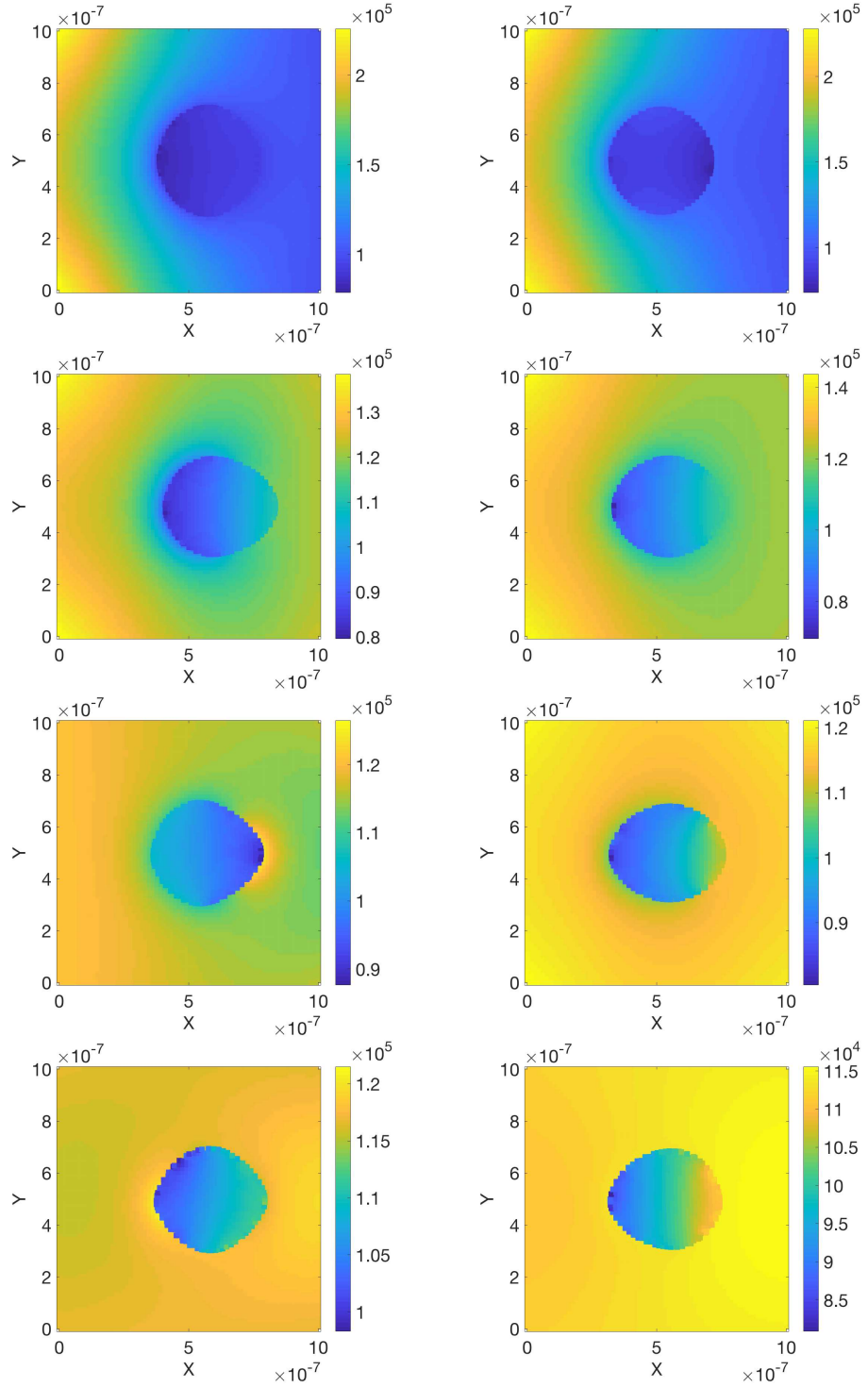


Fig. 4.11: Pressure of gas and liquid at time $t = 2 \cdot 10^{-9}$ (first row), $t = 4 \cdot 10^{-9}$ (second row), $t = 6 \cdot 10^{-9}$ (third row) and $t = 1.4 \cdot 10^{-8}$ (fourth row). Left column: $\rho_l = 2$. Right column: $\rho_l = 10$.

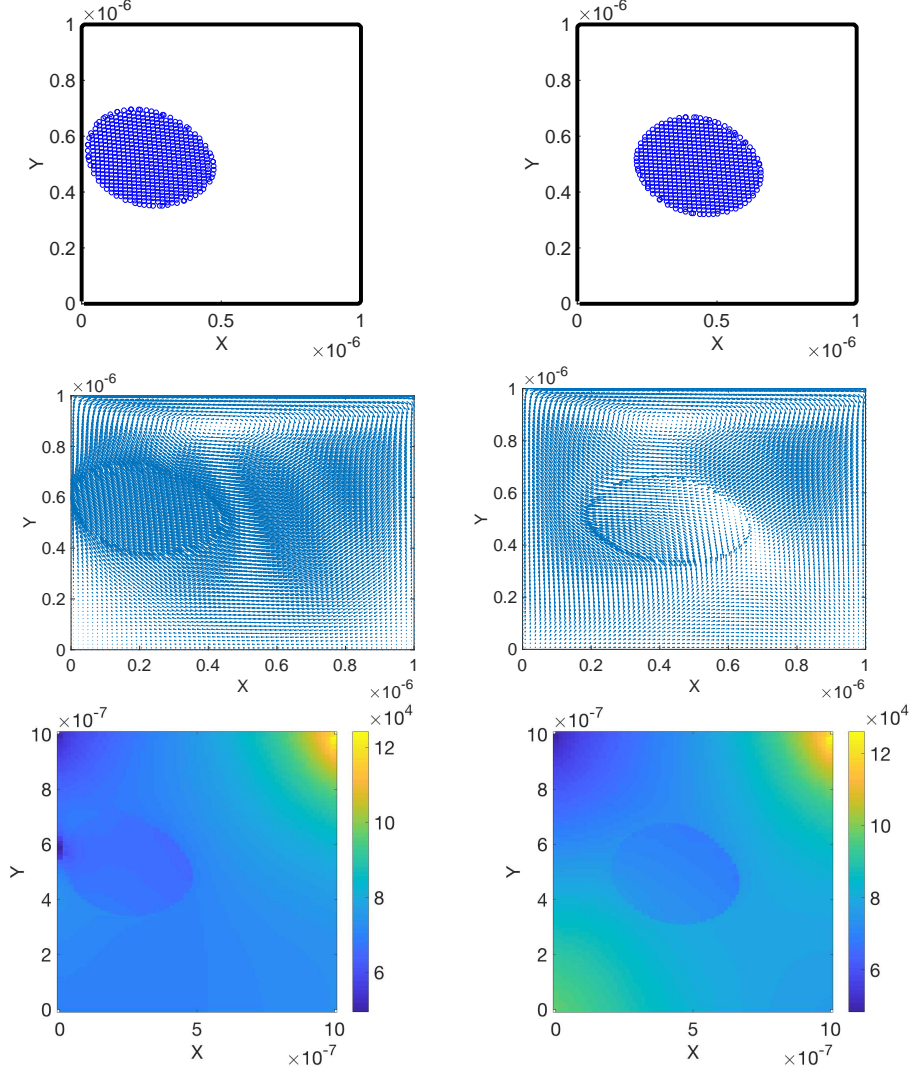


Fig. 4.12: Particle positions of liquid drop (first row), velocity field (second row) and pressure (third row) at time $t = 1.84 \cdot 10^{-8}$. Left column: $\rho_l = 2$. Right column: $\rho_l = 10$.

are applied on all boundaries and on the surface of the liquid drop. The viscosity of the liquid and the surface tension coefficients are the same as before. We have considered an upper wall velocity equal to 30 in the positive x -direction. Figure 4.12 shows the lighter and the heavier drop following the circulation. The simulations are performed until the lighter drop hits one of the walls, when the simulation is stopped for both cases. We observe that the motion of the heavier drop is slower and the lighter drop is slightly more deformed than the heavier one.

5. Conclusion and Outlook. In this paper we have presented 1D and 2D simulations of a moving liquid drop inside a rarefied gas flow. This is a direct extension

of earlier work, where we have presented a moving rigid body immersed in a rarefied gas flow, see [22]. We have considered a two way coupling in which the motion of the gas influences the motion of the liquid and vice versa. The rarefied gas phase is simulated by solving the BGK model of the Boltzmann equation and the liquid phase is simulated by solving the incompressible Navier-Stokes equations. A meshfree method based on the moving least squares approach is applied for both types of equations. The heat exchange between the two phase is not considered. As interface conditions the continuity of velocity and momentum are applied. Numerical results in one and two physical spaces are presented. In the one dimensional case, the results are compared with coupled solutions of Boltzmann and incompressible Navier-Stokes equations, where the Boltzmann equation is solved by a DSMC method. In the two dimensional case two examples are presented. First we considered a moving drop driven by a shock wave. Second a drop immersed in a driven cavity moving along the circulation of the flow is considered. Two density ratios between gas and liquid are investigated, which are $\rho_g : \rho_l = 1 : 2$ and $1 : 10$. For the density ratio $1 : 2$ one observes more deformations and faster movements than for a larger density ratio. Future works will include the heat transfer between two phases and the extension to the three dimensional case.

Acknowledgment. This work is supported by the DFG (German research foundation) under Grant No. KL 1105/30-1 and by the ITN-ETN Marie-Curie Horizon 2020 program ModCompShock, Modeling and computation of shocks and interfaces, Project ID: 642768. G.R. would like to thank the Italian Ministry of Instruction, University and Research (MIUR) to support this research with funds coming from PRIN Project 2017 (No.2017KKJP4X entitled Innovative numerical methods for evolutionary partial differential equations and applications). G. Russo is a member of the INdAM Research group GNCS.

REFERENCES

- [1] G. A. Bird, Molecular Gas Dynamics and Direct Simulation of Gas Flows, Oxford University Press, New York, 1994.
- [2] C. Cercignani, R. Illner, M. Pulvirenti, The Mathematical Theory of Dilute Gases. Springer, 1994.
- [3] S. Chapman, T. W. Cowling, The Mathematical Theory of Non-Uniform Gases, Cambridge University Press, 1970.
- [4] A. J. Chorin, Numerical solution of the Navier-Stokes equations, *Math. Comput.* 22(104) (1968), 745–62.
- [5] C. K. Chu, Kinetic-theoretic description of the formation of a shock wave, *Phys. Fluids* 8 (1965), 12–22.
- [6] G. Dechristé, L. Mieussens Numerical simulation of micro flows with moving obstacles. *Journal of Physics: Conference Series* (2012) 362: 012030.
- [7] G. Dechristé, L. A. Mieussens, Cartesian cut cell method for rarefied flow simulations around moving obstacles. *J. Comput. Phys.* 314 (2016), 454–488.
- [8] P. Degond, G. Dimarco and L. Pareschi, The moment-guided Monte Carlo method, *Int. J. Num. Meth. Fluids*, 67 (2011), 189–213.
- [9] R. Fedkiw, B. Merriman, S. Osher, Numerical methods for a one-dimensional interface separating compressible and incompressible flows. In: *Barriers and challenges in computational fluid dynamics*. Norwell (MA): Kluwer Academic Publishers; 1998. p. 155–94.
- [10] O. Iliev, S. Tiwari, A generalized (meshfree) finite difference discretization for elliptic interface problems. Revised papers from the 5th international conference on numerical methods and applications, NMA '02, pages 488–497. London, UK: Springer-Verlag; 2003.
- [11] A. V. Kityk, K. Knorr, P. Huber, The Development of Free Surface Capturing Approach for Multi Dimensional Free Surface Flows in Closed Containers, *J. Comput. Phys.* 138 (1997), 339–980.

- [12] T. Liszka, J. Orkisz, Special issue-computational methods in nonlinear mechanics the finite difference method at arbitrary irregular grids and its application in applied mechanics. *Comput Struct* 11(1) (1980), 83–95.
- [13] H. Neunzert, J. Struckmeier, *Particle methods for the Boltzmann equation*, Acta Numerica (1995), 417.
- [14] J. M. Oh, T. Faez, S. de Beer, F. Mugele, Capillarity-driven Dynamics of Water-alcohol Mixtures in Nanofluidics Channels, *Microfluid. and Nanofluid* 9 (2010), 123–129.
- [15] Peskin CS (1972) Flow patterns around heart valves: A digital computer method for solving the equations of motion, *PhD thesis*, Albert Einstein College of Medicine.
- [16] V. N. Phan, N.-T. Nguyen, C. Yang, P. Joseph, L. Djeghlaf, D. Bourrier, A.-M. Gue, Capillary Filling in Closed End Nanochannels, *Langmuir* 26 (2010), 3251–1325.
- [17] G. Russo, F. Filbet, Semi-Lagrangian schemes applied to moving boundary problems for the BGK model of rarefied gas dynamics. *Kinet Relat Mod, AIMS* 2 (2009), 231–250.
- [18] Y. Sone, Molecular Gas Dynamics, Theory, Techniques and Applications, Birkhaueser, 2007.
- [19] T. Tsuji, K. Aoki, Moving boundary problems for a rarefied gas: Spatially one dimensional case. *J Comput Phys* 250 (2013), 574–600.
- [20] S. Tiwari, A. Klar, S. Hardt, A particle-particle hybrid method for kinetic and continuum equations, *J. Comp. Phys.* 228 (2009) 7109–7124.
- [21] S. Tiwari, A. Klar, S. Hardt, A. Donkov, Coupled solution of the Boltzmann and Navier–Stokes equations in gas–liquid two phase flow, *Computers and Fluids* 71, (2013) 283–296.
- [22] S. Tiwari, A. Klar, G. Russo, Interaction of rigid body motion and rarefied gas dynamics based on the BGK model, *Mathematics in Engineering*, 2,2, (2020) 203–229.
- [23] S. Tiwari, J. Kuhnert, A meshfree method for incompressible fluid flows with incorporated surface tension, *Revue europeenne des elements finis*, 11, No. 7-8, (2002). (Meshfree and Particle Based approaches in Computational Mechanics).
- [24] S. Tiwari, J. Kuhnert, Modeling of two phase flows with surface tension by Finite Pointset Method (FPM), *J. Comput. Appl. Math* 203 (2007) 376–386.